scientific reports

Check for updates

OPEN

Optimizing entropy generation in MHD Maxwell dusty nanofluid flow via nanoparticle radius and inter-particle spacing on an inclined stretching sheet

Aziz Ullah Awan[1,2], Shafiullah Niazai[3]✉, Muzammil Hussain[1], Bagh Ali[4], N. Ameer Ahammad[5], Fehmi Gamaoun[6] & Sohail Nadeem[7]

This study presents a numerical investigation of entropy generation in a magnetohydrodynamic (MHD) flow of a Maxwell dusty nanofluid over an inclined stretching sheet, with a focused analysis on the previously overlooked parameters of nanoparticle radius and inter-particle spacing. The model incorporates the effects of viscous dissipation and thermal buoyancy on the flow dynamics. The governing partial differential equations are transformed into a system of nonlinear ordinary differential equations via similarity transformations and solved computationally using MATLAB's bvp4c solver, with validation against published results confirming high accuracy. The findings quantitatively show that nanoscale particle geometry is a key factor influencing thermal performance and irreversibility. A reduction in the nanoparticle radius from 3.6 nm to 1.6 nm under standard conditions ($h_p = 0.5$, $\beta = 0.5$, $M = 3.0$) suppresses total entropy generation by approximately 20%. Conversely, increasing the nanoparticle radius beyond 2.5 nm enhances both the fluid and dust phase velocities by nearly 18%, which is beneficial for flow applications, but concurrently reduces the effective thermal conductivity by almost 12% due to a diminished surface-area-to-volume ratio. Furthermore, the analysis shows that increasing inter-particle spacing decreases entropy generation by reducing particle clustering. This study bridges a crucial research gap in the literature by quantifying the role of nanoparticle microstructure. It provides an operational framework for developing high-efficiency, low-irreversible thermal control systems in industries such as advanced manufacturing and energy production.

Keywords Heat transfer, Dusty fluid, Inclined stretching surface, Nanoparticle radius variation, Entropy generation, MHD

Nomenclature

μ_{nf}	Nanofluid dynamic viscosity (Pa s)
$K = 6\pi\mu r$	Stokes' drag constant (kg s^{-1})
σ_{nf}	Nanofluid electrical conductivity (S m^{-1})
C_p	Fluid specific heat at constant pressure (J $kg^{-1}\cdot K^{-1}$)
$\theta(\eta)$	Dimensionless fluid temperature
u_p	Dust particle velocity in x-direction (m s^{-1})
h_p	Inter-particle spacing (m)
E_c	Eckert number (dimensionless)

[1]Institute of Mathematics, University of the Punjab, Lahore 54590, Pakistan. [2]Center for Theoretical Physics, Khazar University, 41 Mehseti Str., Baku AZ1096, Azerbaijan. [3]Department of Mathematics, Education Faculty, Laghman University, Mehterlam City, Laghman 2701, Afghanistan. [4]Department of Mathematical Sciences, Saveetha School of Engineering, SIMATS, Chennai 602105, Tamilnadu, India. [5]Department of Mathematics, Faculty of Science, University of Tabuk, Tabuk, Saudi Arabia. [6]Department of Mechanical Engineering, College of Engineering, King Khalid University, Abha 61421, Saudi Arabia. [7]Department of Mathematics, Quaid-i-Azam University, Islamabad 44000, Pakistan. ✉email: shafiullahniazai@lu.edu.af

v_p	Dust particle velocity in y-direction (m s^{-1})
T_∞	Ambient temperature (K)
N	Number density of dust particles (m^{-3})
M	Magnetic parameter (dimensionless)
β_t	Thermal dusty interaction parameter (dimensionless)
$f'(\eta)$	Dimensionless fluid velocity
Re_x	Reynolds number (dimensionless)
C_{f_x}	Skin friction coefficient (dimensionless)
Ns	Entropy generation number (dimensionless)
ρ_{nf}	Nanofluid density (kg m^{-3})
B_0	Uniform magnetic field (T)
τ_T	Thermal equilibrium time (s)
c_m	Dust particle specific heat (J $kg^{-1}\cdot K^{-1}$)
$\theta_p(\eta)$	Dimensionless dust temperature
u	Fluid velocity in x-direction (m s^{-1})
d_p	Nanoparticle radius (m)
β	Maxwell parameter (dimensionless)
v	Fluid velocity in y-direction (m s^{-1})
m	Dust particle mass (kg)
λ	Thermal conductivity (W $m^{-1}\cdot K^{-1}$)
Pr	Prandtl number (dimensionless)
γ_t	Specific heat ratio (dimensionless)
$f_p(\eta)$	Dimensionless dust velocity
u_w	Stretching velocity of sheet (m s^{-1})
Nu_x	Nusselt number (dimensionless)
Be	Bejan number (dimensionless)

Literature review

Entropy generation, as a measure of irreversibility and disorder in thermodynamic systems, is a key factor in energy transfer efficiency. It has been extensively investigated in various applications, including electronics, solar systems, and heat exchangers. Bejan[1–3] introduced the idea of entropy optimization in the context of mass and heat transfer phenomena. Razaq et al.[4] examined entropy optimization in Reiner-Rivlin nanomaterial fluid flow caused by a stretchable cylinder underlying MHD and chemical reactions. Sahoo and Nandkeolyar[5] studied MHD flow of Casson nanofluid with entropy, chemical reactions, activation energy, and Hall current over a stretchable surface in porous media. Khan et al.[6] scrutinized a thermally conductive nanofluid flow across a curved stretchable sheet with the Darcy-Forchheimer relation.

The dusty fluid flow occurs when solid particles are distributed in the fluid. The dusty fluid flow is utilized in paint spraying, gas-freezing systems, nuclear reactor cooling, and dust collection. Saffman[7] presented the basic concept of dusty fluids and derived constitutive equations based on Stokes' law of drag forces. His research demonstrated that the thermal transmission rate is enhanced by suspending dusty particles. Ezzat et al.[8] investigated free-convective thermal transfer in a dusty fluid flow caused by a vertically positioned plate in a permeable medium under an applied magnetic field. Abbas et al.[9] provided analytical and numerical solutions for a magnetized dusty fluid flow across a stretched permeable sheet, considering slip conditions. Dey and Chutia[10] studied the bioconvective dusty nanofluid flow over a vertically stretched flat surface. Sharif et al.[11] employed a numerical method, bvp4c, to probe a dusty trihybrid Ellis nanofluid flow across an expanding Riga plate.

Alfvén[12], a Nobel laureate, investigated the magnetic properties of electrically conducting fluids in the presence of a steady magnetic field. He demonstrated how fluid movement induces an electromotive force, generating an electric current. Given their potential uses in cosmology, astronomy, medicine, engineering, and industry, MHD fluids have garnered special scientific attention. Hayat et al.[13] investigated the MHD flow and heat transfer characteristics of permeable stretched sheets, taking into account slip effects. Kumar et al.[14] investigated numerically the MHD dusty fluid flow across an stretched sheet using fluid-particle suspension. MHD dusty Casson fluid flow over a stretching sheet has been demonstrated by Gireesha et al.[15] by applying Fourier law along with Cattaneo-Christov heat flux law. Ali et al.[16] investigated incompressible MHD dusty Casson nanofluid flow between two plates using the perturbation method.

Choi and Eastman[17] introduced the concept of dispersing nanoparticles in a base fluid. Nanofluids have better thermal performance than traditional fluids[18]. Common base fluids include water, oil, and biofluids, while nanoparticles can be metals, oxides, or carbides. Nanofluids are used in a wide range of industries, including biomedical fields like drug delivery, cancer hyperthermia, monitoring heart function, and blood temperature control[19]; industrial processes like lubrication, chemical processing, and MHD pumping; energy systems including solar collectors, nuclear reactors, and geothermal reservoirs for improved heat extraction; electronics cooling for microprocessors, sensors, and power devices; and automobile engines for enhanced efficiency[20]. Studies on nanofluid convection using the lattice Boltzmann method include Alinejad and Esfahani[21] in D3Q19 enclosures, Araban et al.[22] for CuO-water nanofluids, and Sahebi et al.[23] on nanofluid flow over cylinders.

Many theoretical calculations and experiments have been conducted to determine the mechanisms that enhance the thermal conductivity of nanofluids. This enhancement is attributed to the characteristics of the base fluid and the nanoparticles. Key characteristics of nanofluids include nanoparticle radius, friction factor, and nanoparticle concentration. Timofeeva et al.[24] highlighted nanoparticle radius as one of the most critical factors in improving heat transmission. Nanoparticle radius variation alters the inherent magnetic properties, impacting fluid behavior. Specifically, superparamagnetic behavior changes with a change in nanoparticle radius.

The effect of particle size variation on oil transmission in pipelines using the D2Q9 lattice Boltzmann method was reported by Madani et al.[25]. Hussain et al.[26] emphasized the significance of nanoparticle radius variation in nanofluid flow past a stretched surface.

Significance of the study

Understanding entropy generation in dusty fluid and nanofluid flows is vital for increasing energy efficiency and thermal control in engineering systems. Nanoparticles enhance heat conductivity, while dust particles facilitate heat and momentum exchange, making dusty nanofluids attractive for applications such as electronic cooling, heat exchangers, and energy storage. When combined with magnetohydrodynamics (MHD), their relevance extends to metallurgical processes, nuclear reactors, and biological systems, where efficient heat transfer with minimal irreversibility is vital.

Research gap

Despite extensive progress, most studies have investigated entropy either in MHD dusty flows or traditional nanofluids. The influence of essential factors, nanoparticle radius and inter-particle spacing, which directly control thermal conductivity, dustâ€"fluid interaction, and entropy production, has received little attention. Table 1 summarizes existing contributions and highlights the overlooked dimension. To fill this gap, the current study focuses on these nanoscale parameters while numerically investigating entropy generation in MHD Maxwell dusty nanofluid flow over an inclined stretching sheet.

Novelty and contributions

This study advances the field by systematically quantifying the role of nanoparticle radius and inter-particle spacing on the flow, entropy production, and thermal efficiency in dusty nanofluids. The study focuses on reducing energy loss and improving heat transfer across a wide range of applications, including cooling technologies, energy systems, and manufacturing processes. The key novelties of the study include:

- Development of Maxwell dusty nanofluid model integrating both dust particles and nanoparticles.
- Systematic evaluation of nanoparticle radius and inter-particle spacing on thermal conductivity, flow dynamics, and entropy.
- Extension of fluid-particle interaction models by including MHD effects across an inclined stretching sheet.
- Inclusion of viscous dissipation and thermal buoyancy to simulate realistic transport phenomena.

By offering new insights into the characteristics of nanoscale particles that govern thermal conductivity, this framework enables the creation of more effective thermal systems that lose less energy.

Flow analysis

Mathematical model

A mathematical formulation is developed to investigate fluid dynamics, heat transfer, and entropy optimization in a steady, two-dimensional dusty nanofluid flow across an inclined, stretched surface. The flow assumptions are as follows:

- Dust and nanoparticles are dispersed in the Maxwell fluid.
- The stretching sheet is inclined at an angle α to the vertical.
- Dust particles are spherical, evenly sized, and equally dispersed in Maxwell nanofluid.
- The density of dust particles and nanoparticles remains constant throughout the incompressible steady fluid flow.
- Agglomeration or accumulation of nanoparticles is neglected.
- A uniform magnetic field strength B_0 is applied normally to the stretched sheet.
- Ohmic dissipation, ion-slip effects, and Hall current are ignored due to a weak magnetic field[26].
- The sheet surface stretches with velocity $u_w = ax$ along the x-axis.

The flow configuration is illustrated in Fig. 1. Following[26,32–34], the governing equations for the present flow are:

Authors	Maxwell fluid	Nanoparticles	Tiwari-Das model	Dust particles	Nanoparticle radius impact	Thermal buoyancy	Role of inter-particle spacing	Entropy analysis
Hussain et al.[26]	✗	✓	✓	✓	✓	✗	✗	✗
Ali et al.[27]	✗	✓	✓	✗	✓	✓	✗	✗
Ali et al.[28]	✓	✗	✗	✓	✗	✓	✗	✓
Darvesh et al.[29]	✗	✓	✓	✗	✓	✗	✓	✗
Ramzan et al.[30]	✗	✓	✓	✗	✓	✗	✓	✗
Algehyne[31]	✗	✓	✓	✗	✓	✗	✓	✓
Current study	✓	✓	✓	✓	✓	✓	✓	✓

Table 1. Existing research gap and contributions of the current study.

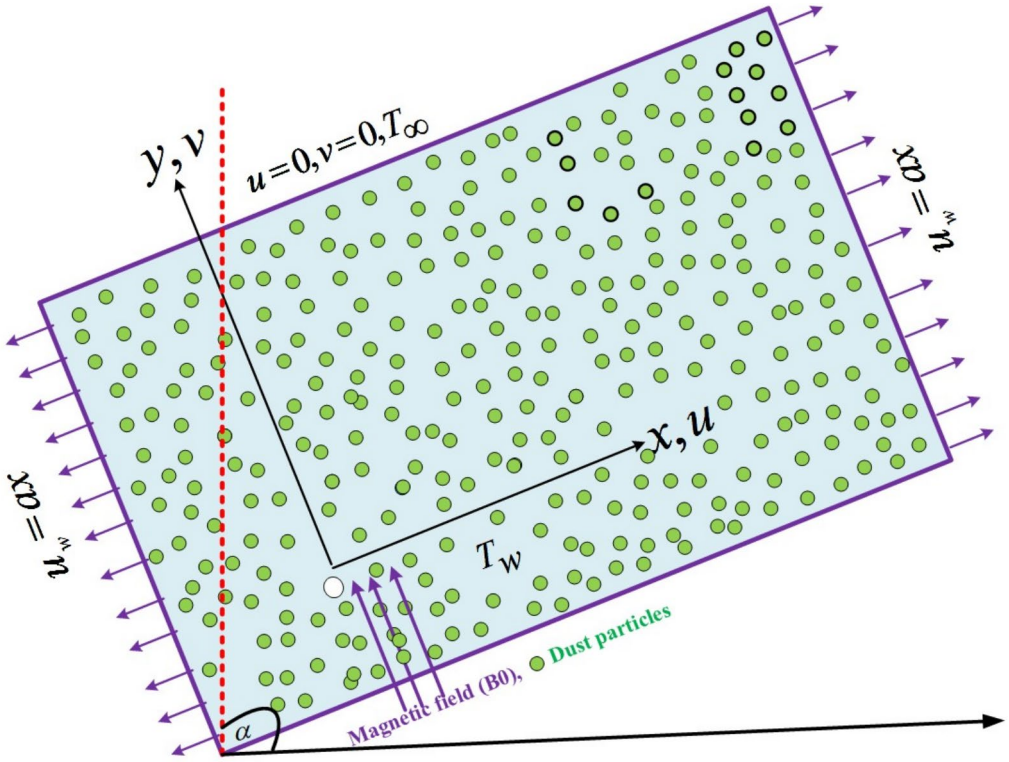

Fig. 1. Schematic flow configuration.

$$\frac{\partial u}{\partial x}+\frac{\partial v}{\partial y}=0, \tag{1}$$

$$u\frac{\partial u}{\partial x}+v\frac{\partial u}{\partial y}+\lambda_1\left(u^2\frac{\partial^2 u}{\partial x^2}+v^2\frac{\partial^2 u}{\partial y^2}+2uv\frac{\partial^2 u}{\partial x\partial y}\right)=\frac{\mu_{nf}}{\rho_{nf}}\frac{\partial^2 u}{\partial y^2} +g\frac{(\check{\beta}_0\rho)_{nf}}{\rho_{nf}}(T-T_\infty)cos\alpha-\frac{\sigma_{nf}B_0^2u}{\rho_{nf}}+\frac{KN}{\rho_{nf}}(u_p-u), \tag{2}$$

$$(\rho c_p)_{nf}\left[u\frac{\partial T}{\partial x}+v\frac{\partial T}{\partial y}\right]=k_{nf}\frac{\partial^2 T}{\partial y^2}+\mu_{nf}\left(\frac{\partial u}{\partial y}\right)^2+\frac{C_p\rho_p}{\tau_T}(T_p-T). \tag{3}$$

For dust particle flow:

$$\frac{\partial u_p}{\partial x}+\frac{\partial v_p}{\partial y}=0, \tag{4}$$

$$u_p\frac{\partial u_p}{\partial x}+v_p\frac{\partial u_p}{\partial y}=\frac{KN}{\rho}(u-u_p), \tag{5}$$

$$u_p\frac{\partial T_p}{\partial x}+v_p\frac{\partial T_p}{\partial y}=\frac{c_p}{c_m\tau_T}(T-T_p). \tag{6}$$

Here, u and v denote velocity components along $x-$ and $y-$axes, while u_p and v_p represent the corresponding components of dust phase velocity. T_w and T_∞ indicate the boundary and ambient temperatures, respectively; g is the gravitational acceleration; N the dust particle number density; and B_0 the applied magnetic field strength. The nanofluid properties are characterized by viscosity μ_{nf} and density ρ_{nf}. T_p and c_m correspond to the temperature and specific heat of dusty fluid, respectively, while K represents the Stokes' drag constant.

Term-wise interpretation of equations

The governing equations characterize the coupled transport phenomena in incompressible dusty nanofluid flow. The continuity equation (1) enforces mass conservation in the carrier-particle mixture[32]. In Eq. (2), the left-hand side accounts for the convective acceleration of base fluid together with the viscoelastic stresses introduced by the Maxwell fluid model. On the right-hand side, the first term represents viscous momentum diffusion within the boundary layer[35], while the second term captures buoyancy-driven natural convection arising from

density gradients[38]. The third term, associated with the Lorentz force, expresses magnetic damping of motion in line with classical MHD theories[36,37]. The final term establishes fluid-particle coupling, representing drag exerted by the dust phase on the carrier fluid[15]. The energy equation (3) represents the thermal energy balance in the dusty nanofluid system. The left-hand side describes how heat is carried by the moving nanofluid, which is essentially the transport of energy via convection as the fluid flows[35]. The first term on the right-hand side represents the conduction of heat within the fluid, which is further enhanced by the nanoparticles' addition in the effective thermal conductivity[26]. The following term illustrates how heat is generated internally by the fluid's motion; viscous dissipation is the process by which fluid layers slide past one another, and frictional forces convert kinetic energy into thermal energy[39]. The final term refers to the direct heat exchange between dust particles and fluid[15]. This interaction is essential because it permits the particulate phase to affect the thermal field. Equations (4–6) are governing equations for the flow of dusty phase[26]. Equation (4) ensures conservation of dust particle mass within the flow field. Equation (5) represents the momentum balance for dust particles, which is determined by drag attraction with the surrounding fluid. Equation (6) describes the energy balance of dust particles, emphasizing the heat exchange between the particle and fluid phases.

Boundary conditions

The present model focuses on the combined effects of dust particles, nanoparticles, thermal buoyancy, magnetic fields, and viscous dissipation on flow dynamics, entropy generation, and heat transfer in a Maxwell dusty nanofluid flow over an inclined stretching sheet. The following boundary conditions represent the physical constraints of boundary layer fluid flow[26,35]:

$$\begin{cases} u = u_w = ax, \quad v = 0, \quad T = T_w, \quad \text{as} \quad y = 0, \\ u \to 0, \quad v = v_p \to 0, \quad T \to T_\infty, \quad u_p \to 0, \quad T_p \to T_\infty, \quad \text{as} \quad y \to \infty. \end{cases} \tag{7}$$

Thermophysical properties of nanofluid

The effective properties of nanofluid are expressed in Table 2 as stated by[35,40,41].

Here, ϕ is the solid volume fraction, while subscripts f and s correspond to the base fluid and nanoparticles, respectively. The radius of the nanoparticle and the inter-particle spacing are represented by d_p and h_p, respectively.

Similarity variables

Similarity variables are introduced as[42–44]:

$$\begin{cases} \eta = \sqrt{\frac{a}{\nu_f}}y, \quad v = -\sqrt{a\nu_f}f(\eta), \quad u = axf'(\eta), \quad \theta(\eta) = \frac{T-T_\infty}{T_w-T_\infty}, \\ u_p = axf_p'(\eta), \quad v_p = -\sqrt{a\nu}f_p(\eta), \quad \theta_p(\eta) = \frac{T_p-T_\infty}{T_w-T_\infty}. \end{cases} \tag{8}$$

Dimensionless system

Using Eq. (8), Eqs. (1) and (4) are satisfied automatically. Other equations reduce to:

$$\frac{A_1}{A_2}f''' - f'^2 + ff'' + \beta(2f''f'f - f^2f''') + \frac{A_6}{A_2}\lambda\theta cos\alpha + \frac{\Gamma_v\beta_v}{A_2}\left(f_p' - f'\right) - \frac{A_3}{A_2}Mf' = 0, \tag{9}$$

$$\frac{A_4}{A_5}\theta'' + Prf\theta' + \frac{1}{A_5}Pr\gamma_t\beta_t\left(\theta_p - \theta\right) + PrE_cf''^2 = 0, \tag{10}$$

$$f_p'^2 + \beta_v\Gamma_v\left(f_p' - f'\right) - f_pf_p'' = 0, \tag{11}$$

Effective property of nanofluid	Parameter
Viscosity	$\frac{\mu_{nf}}{\mu_f} = 1 + 2.5\phi + 4.5\left[\frac{1}{\frac{h_p}{d_p}(2+\frac{h_p}{d_p})(1+\frac{h_p}{d_p})^2}\right]$
Thermal expansion	$\frac{(\rho\check{\beta}_0)_{nf}}{(\rho\check{\beta}_0)_f} = (1-\phi) + \phi\frac{(\rho\beta_0)_s}{(\rho\beta_0)_f}$
Electrical conductivity	$\frac{\sigma_{nf}}{\sigma_f} = 1 + \frac{3\left(\frac{\sigma_s}{\sigma_f}-1\right)\phi}{\left(\frac{\sigma_s}{\sigma_f}+2\right)-\left(\frac{\sigma_s}{\sigma_f}-1\right)\phi}$
Thermal conductivity	$\frac{k_{nf}}{k_f} = \frac{k_s+2k_f-2\phi(k_f-k_s)}{k_s+2k_f+\phi(k_f-k_s)}$
Density	$\frac{\rho_{nf}}{\rho_f} = 1 - \phi + \phi\frac{\rho_s}{\rho_f}$
Heat capacity	$\frac{(\rho C_p)_{nf}}{(\rho C_p)_f} = 1 - \phi + \phi\frac{(\rho C_p)_s}{(\rho C_p)_f}$

Table 2. Effective properties of nanofluid[35,40,41].

$$f_p\theta_p' + \beta_t\gamma_t\,(\theta - \theta_p) = 0, \tag{12}$$

while the boundary constraints take the form:

$$\begin{cases} f(0) = 0,, & f'(0) = 1, & \theta(0) = 1, \\ f_p'(\infty) \to 0, & f'(\infty) \to 0, & f_p(\infty) = f(\infty) \to 0, \quad \theta_p(\infty) \to 0, \quad \theta(\infty) \to 0. \end{cases} \tag{13}$$

Dimensionless parameters

Here, *Pr* is the Prandtl number, λ the thermal buoyancy parameter, and E_c the Eckert number. Fluid-temperature interaction, specific heat ratio, the mass concentration of dusty granules, and fluid particle interaction for velocity are expressed by β_t, γ_t, Γ_v, and β_v, respectively. These dimensionless numbers are mathematically defined as:

$$\begin{cases} A_1 = \frac{\mu_{nf}}{\mu_f} = 1 + 2.5\phi + 4.5\left[\frac{1}{\frac{h_p}{d_p}(2+\frac{h_p}{d_p})(1+\frac{h_p}{d_p})^2}\right], \ \lambda = \frac{g\beta_T^* x(T_w - T_\infty)}{u_w^2}, \\ \Gamma_v = \frac{Nm}{\rho}, \quad \beta = a\lambda_1, \quad \beta_v = \frac{1}{a\tau_v}, \quad \beta_t = \frac{1}{a\tau_t}, \quad E_c = \frac{u_w^2}{(T_w - T_\infty)C_p}, \\ A_4 = \frac{k_{nf}}{k_f} = \frac{k_s + 2k_f - 2\phi(k_f - k_s)}{k_s + 2k_f + \phi(k_f - k_s)}, \quad A_2 = \frac{\rho_{nf}}{\rho_f} = 1 - \phi + \phi\frac{\rho_s}{\rho_f}, \\ \gamma_t = \frac{c_p}{c_m}, \quad Pr = \frac{\mu_f C_p}{k_f}, \quad A_3 = \frac{\sigma_{nf}}{\sigma_f} = 1 + \frac{3\left(\frac{\sigma_s}{\sigma_f} - 1\right)\phi}{\left(\frac{\sigma_s}{\sigma_f} + 2\right) - \left(\frac{\sigma_s}{\sigma_f} - 1\right)\phi}, \\ M = \frac{\sigma_f B_0^2}{a\rho_f}, \quad A_6 = \frac{(\check{\beta}_0\rho)_{nf}}{(\check{\beta}_0\rho)_f}, \quad A_5 = \frac{(\rho C_p)_{nf}}{(\rho C_p)_s} = 1 - \phi + \phi\frac{(\rho C_p)_s}{(\rho C_p)_{nf}}. \end{cases} \tag{14}$$

To improve clarity, Table 3 summarizes the definitions, physical significance, and potential uses of the essential dimensionless parameters employed in this work.

Engineering quantities

The local skin friction coefficient Cf_x and Nusselt number Nu_x are given as[26,43]:

$$Cf_x = \frac{\tau_w}{\rho_f (u_w)^2}, \qquad Nu_x = \frac{x q_w}{k_f\,(T_w - T_\infty)}. \tag{15}$$

Wall shear stress is $\tau_w = \mu_{nf}\frac{\partial u}{\partial y}\Big|_{y=0}$ and the wall heat flux is $q_w = -k_{nf}\frac{\partial T}{\partial y}\Big|_{y=0}$.

In dimensionless form, the local skin friction coefficient and Nusselt number are expressed as:

$$\sqrt{Re_x}Cf_x = A_1 f''(0), \qquad \frac{1}{\sqrt{Re_x}}Nu_x = -A_4\theta'(0), \tag{16}$$

where $Re_x = \frac{u_w x}{\nu_f}$ shows local Reynolds number.

Solution procedure

The governing PDEs (1–6) along with boundary conditions (7) are first transformed into a set of nonlinear ODEs (9–12) with corresponding transformed constraints (13) using the similarity transformation defined in Eq. (8). These resulting ODEs are highly nonlinear, making exact solutions intractable. Therefore, a numerical technique is adopted. Numerical methods provide adaptability and flexibility, enabling the practical solution of complicated problems. Ensuring high numerical accuracy is critical to guarantee that the computed results closely approximate the actual physical behavior. Among different methods, MATLAB's bvp4c solver is selected

Parameters	Definition/Physical Significance	Applications
Pr	The relative thickness of the velocity and thermal boundary layers is indicated by the ratio of momentum diffusivity to thermal diffusivity.	Heat exchangers, thermal insulation, polymer manufacturing, and electronic device cooling.
E_c	Viscous dissipation effects are measured by the ratio of kinetic energy to enthalpy.	Polymer processing and nanofluid energy systems.
β	The fluid's viscoelastic properties are described by the Maxwell relaxation parameter.	Viscoelastic fluid modeling, polymer melts, and non-Newtonian fluid flows.
d_p	The radius of the nanoparticle affects the thermophysical characteristics of the nanofluid via influencing thermophoretic diffusion and Brownian motion.	Advanced heat transfer systems, thermal energy storage, and microfluidics.
M	Lorentz force effects on electrically conducting fluids are measured by the magnetic parameter.	MHD generators, plasma control, electromagnetic pumps, and nuclear reactor cooling.
λ	The thermal buoyancy parameter measures the impact of temperature gradient-induced buoyant forces.	Applications for natural convection, material processing, solar collectors, and crystal formation.
h_p	Inter-particle spacing affects flow dynamics and thermal conductivity via regulating nanoparticle interactions and distribution.	Energy systems, microchannel heat transmission, and nanofluid design.

Table 3. Interpretation and applications of key dimensionless parameters.

due to its robust handling of boundary value problems. The bvp4c solver combines the shooting method, collocation, and adaptive mesh refinement.

To employ bvp4c, the following fresh variables are defined to express the nonlinear system (9–12) as first-order ODEs:

$$f = s_1, f' = s_2, f'' = s_3, \theta = s_4, \theta' = s_5, f_p = s_6, f_p' = s_7, \text{ and } \theta_p = s_8.$$

This introduction reduces the system of ODEs to

$$ss1 = \frac{A_2\Big[-s_1 s_3 + {s_2}^2 - 2\beta s_1 s_2 s_3 - s_4 \lambda \frac{A_6}{A_2} cos\alpha - \frac{\Gamma_v \beta_v}{A_2}(s_7 - s_2) + \frac{A_3}{A_2} M s_2\Big]}{A_1 - A_2 \beta {s_1}^2}, \tag{17}$$

$$ss2 = -\frac{A_5}{A_4} Pr\Big[s_1 s_5 + \frac{\gamma_t \beta_t}{A_5}(s_8 - s_4) + E_c {s_3}^2\Big], \tag{18}$$

$$ss3 = \frac{1}{s_6}\Big[s_7^2 + \beta_v \Gamma_v (s_7 - s_2)\Big], \tag{19}$$

$$ss4 = \frac{\beta_t \gamma_t (s_8 - s_4)}{s_6}. \tag{20}$$

The transformed dimensionless boundary constraints are written as:

$$\begin{cases} s_1 = 0, \quad s_2 = 1, \quad s_4 = 1, \quad \text{as} \quad \eta = 0, \\ s_7 \to 0, \quad s_2 \to 0, \quad s_8 \to 0, \quad s_6 = s_1 \to 0, \quad s_4 \to 0, \quad \text{as} \quad \eta \to \infty. \end{cases} \tag{21}$$

By progressively modifying missing initial estimations at $\eta = 0$ to meet the far-field conditions at a sufficiently large but finite $\eta_{\max}$, the bvp4c solver efficiently handles these boundary conditions. To ensure convergence within the boundary layer, the computational domain $[0, \eta_{\max}]$ is selected so that any increments in $\eta_{\max}$ do not substantially alter the solution. The stopping criterion is defined as:

$$\max\{|s_2(\eta_{\max}) - 0|, |s_1(\eta_{\max}) - 0|, |s_4(\eta_{\max}) - 0|, |s_7(\eta_{\max}) - 0|, |s_8(\eta_{\max}) - 0|, |s_6(\eta_{\max}) - 0|\} < \chi,$$

where $\chi = 10^{-6}$ ensures high precision convergence. This method preserves stability and numerical precision while enabling the methodical study of parameter effects such as magnetic field strength, viscous dissipation, and nanoparticle radius.

Irreversibility analysis

Entropy generation is linked to energy waste, so our primary goal is to minimize entropy production. Measuring entropy generation can help us understand the reasons behind potential system failures. It is analogous to discovering faults in a process or design, allowing us to improve overall performance once these areas are identified. Many industrial and technological sectors strive to improve efficiency by minimizing the generation of entropy. The depletion of global energy resources has prompted experts to examine energy generation designs, conversion, and application. The entropy generation rate per unit volume S_{gen}''' within the context of a magnetic field being present is calculated as follows[39]:

$$S_{gen}''' = \frac{k_{nf}}{T_\infty^2}(\nabla T)^2 + \frac{1}{T_\infty}\left[(\mathrm{J} - \mathrm{QV}) \times (\mathrm{E} + \mathrm{V} \times \mathrm{B})\right] + \frac{\mu_{nf}}{T_\infty}\Phi. \tag{22}$$

Φ, ∇, and J stand for viscous dissipation, Del operator, and current density, respectively. Assuming negligible effects of QV and E compared to magnetic term $\mathrm{V} \times \mathrm{B}$, and applying boundary layer approximation, this reduces to

$$S_{gen}''' = \frac{\mu_{nf}}{T_\infty}\left(\frac{\partial u}{\partial y}\right)^2 + \frac{k_{nf}}{T_\infty^2}\left(\frac{\partial T}{\partial y}\right)^2 + \frac{1}{T_\infty}\left(B_0^2 \sigma_{nf} u^2\right). \tag{23}$$

Three different causes of entropy creation can be seen in this equation. First is heat transmission, which results from the temperature gradient of the problem. Viscous dissipation is the second source arising from fluid friction. Lastly, the most important source is the magnetic force, which results in irreversible Joule dissipation. The volumetric entropy generation rate is represented by entropy generation number *Ns*, defined as the ratio of S_{gen}''' and characteristic entropy generation, S_0'''. From the use of similarity variables, Eq. (23) becomes

$$Ns = \frac{S_{gen}'''}{S_0'''} = A_4 \theta'^2 + Pr E_c \Omega A_1 f''^2 + A_3 M Pr E_c \Omega f'^2, \tag{24}$$

where $\Omega = \frac{T_\infty}{T_w - T_\infty}$ is dimensionless temperature parameter, and $S_0''' = \frac{k_f a}{\Omega^2 \nu_f}$ is characteristic entropy generation. Bejan number is defined as:

M	$\beta_v = 0$			$\beta_v = 0.5$		
	Jalil et al.[45]	Rahman et al.[46]	Our Results	Jalil et al.[45]	Rahman et al.[46]	Our Results
0.2	1.095445	1.0955	1.09548	1.126114	1.1261	1.12610
0.5	1.224745	1.2248	1.22475	1.252251	1.2523	1.25227
1.0	1.414214	1.4142	1.41421	1.438101	1.4381	1.438105
1.5	1.581139	1.5901	1.58857	1.602540	1.6026	1.60258
2.0	1.732051	1.8301	1.83002	1.751609	1.7517	1.75172

Table 4. Comparing the skin friction coefficient with Jalil et al.[45] and Rahman et al.[46] for different values of β_v and M while ignoring all other parameters.

λ	$E_c = 1, Pr = 0.7, M = 1, \alpha = \frac{\pi}{4}$		Pr	$E_c = 1, \lambda = 0.2, M = 1, \alpha = \frac{\pi}{4}$	
	Afridi et al.[39]	Our Results		Afridi et al.[39]	Our Results
0.0	0.5546	0.55465	0.3	0.3897	0.37885
0.5	0.6976	0.69752	0.7	0.6219	0.62176
1.0	0.7931	0.79297	1.2	0.8106	0.82024
1.5	0.8974	0.89744	1.5	0.8962	0.89624

Table 5. Comparing Nusselt number with Afridi et al.[39] for different values of λ and Pr.

$$Be = \frac{\text{Heat transfer irreversibility}}{\text{Total irreversibility}}. \tag{25}$$

By using Eq. (8), we get

$$Be = \frac{A_4 \theta'^2}{Ns}. \tag{26}$$

Results and discussion

This research investigates thermal management and entropy generation in MHD Maxwell dusty nanofluid flow over an inclined stretching surface, focusing on the effects of nanoparticle radius, inter-particle spacing, viscous dissipation, and thermal buoyancy forces. The governing PDEs are converted to nonlinear ODEs using similarity variables and solved numerically via MATLAB's bvp4c solver. Numerical results are validated against published research for limiting cases. The impacts of key significant parameters on the velocity, temperature, Bejan number, and entropy generation are analyzed. Default values of utilized parameters are: $M = 3$, $\beta = 0.5$, $E_c = 0.2$, $\alpha = 45^\circ$, $\lambda = 1.0$, $\beta_v = 0.2$, $\beta_t = 0.1$, $\gamma_t = 0.1$, $\Gamma_v = 0.2$, $h_p = 0.5$, and $d_p = 2.5$.

Numerical validation

Analytical solutions are unavailable due to the coupled nonlinear nature of the equations. Therefore, a numerical validation is needed to establish reliability. The present approach is validated against existing benchmark research in the literature. Tables 4 and 5 compare our results to those given by Jalil et al.[45], Rahman et al.[46], and Afridi et al.[39]. The agreement is excellent, with minimal deviations for different parameters.

Velocity fields

Figure 2 illustrates that raising the Maxwell parameter (β) and magnetic parameter (M) reduces the velocities in both fluid and dust phases. Mechanistically, stronger magnetic fields induce Lorentz forces that oppose the flow, while increased elasticity (larger β) increases internal fluid resistance, slowing momentum transmission. Figure 3 reveals that increasing nanoparticle radius d_p exerts a decisive influence on momentum transport by modulating the effective viscosity. While smaller particles and shorter inter-particle distances exacerbate agglomeration, increase microstructural interactions, and obstruct flow, larger nanoparticles reduce viscous resistance and promote smoother fluid motion. Quantitatively, enlarging the nanoparticle radius from 2.0 nm to 3.0 nm at a fixed spacing of $h_p = 0.5$ results in an approximately 18% increase in the peak velocity of both the fluid and dust phases, confirming the direct link between viscosity reduction, particle radius, and flow acceleration. This behavior highlights the importance of nanoparticle radius and spacing in controlling rheological properties, as higher flow speeds and momentum transfer within the carrier fluid are directly correlated with decreased effective viscosity, with implications for pipeline and microfluidic cooling applications.

Temperature fields

Figures 4, 5, 6 depict the impact of β, M, β_t, E_c, nanoparticle radius (d_p), and inter-particle spacing (h_p) on temperature fields of fluid and dust phases. Figure 4 shows that increased M thickens the thermal boundary layer due to Lorentz force-induced Joule heating. Figure 5 illustrates how the size of nanoparticle radius and inter-

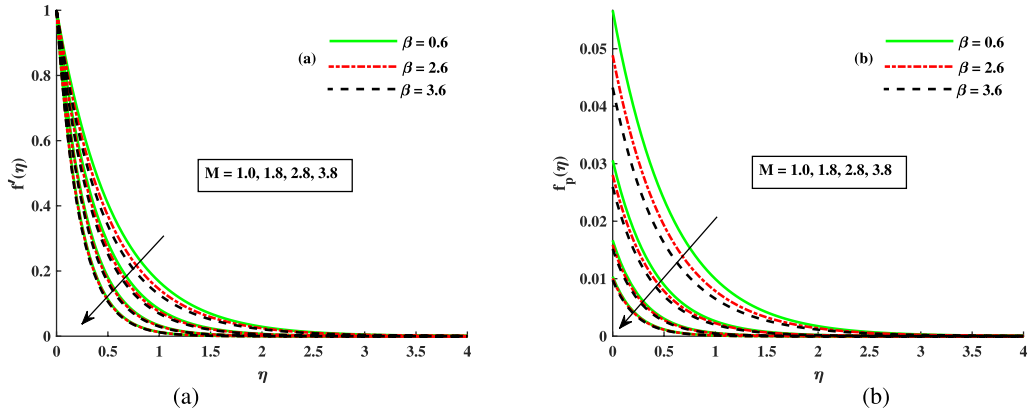

Fig. 2. Response of $f_p(\eta)$ and $f'(\eta)$ for fluctuating β and M.

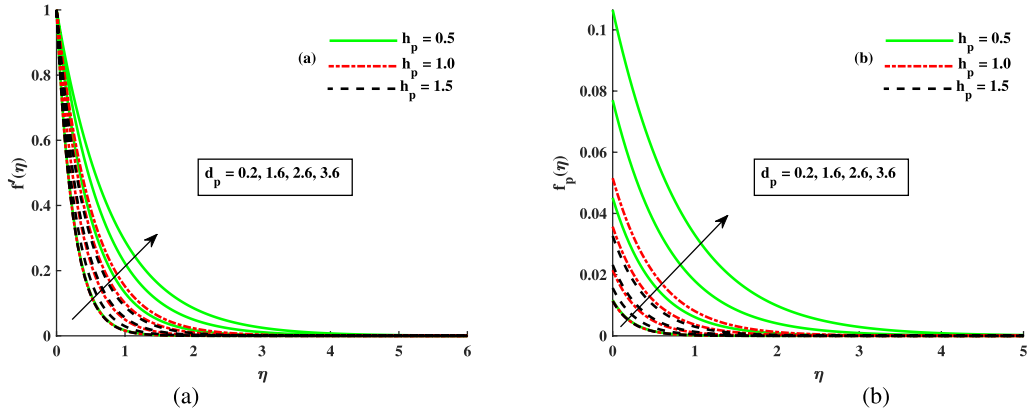

Fig. 3. Response of $f_p(\eta)$ and $f'(\eta)$ for fluctuating h_p and d_p.

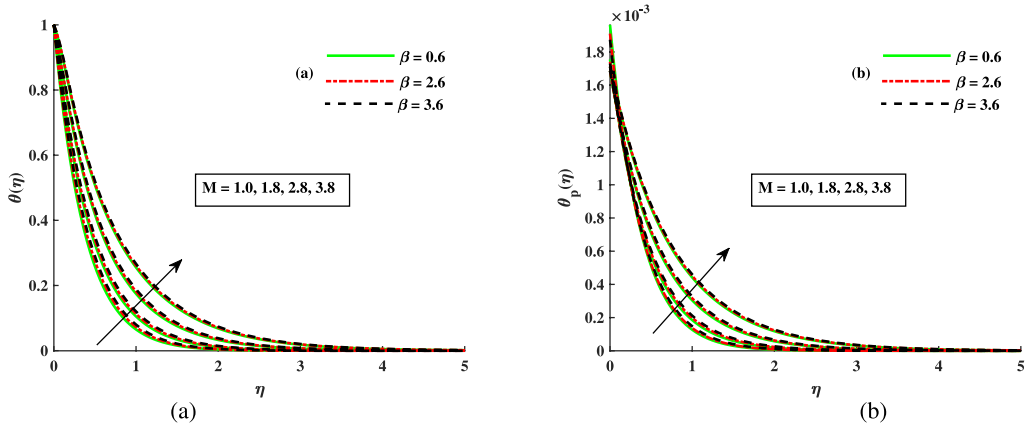

Fig. 4. Response of $\theta(\eta)$ and $\theta_p(\eta)$ for fluctuation of M and β.

particle spacing significantly influence the properties of thermal transport. Due to their lower surface-area-to-volume ratios, larger nanoparticles attenuate temperature gradients within the fluid and reduce the effective thermal conductivity by suppressing heat exchange. Smaller inter-particle spacing, on the other hand, increases phonon scattering, micro-convective interactions, and particle clustering, all of which support localized heat retention. Larger d_p improves hydrodynamic performance, but this is offset by thermal inefficiency: according to the thermophysical mathematical models, an increase in d_p from 2.0 nm to 3.0 nm reduces the effective thermal conductivity by approximately 12%. Figure 6 highlights the effects of thermal dusty parameter β_t

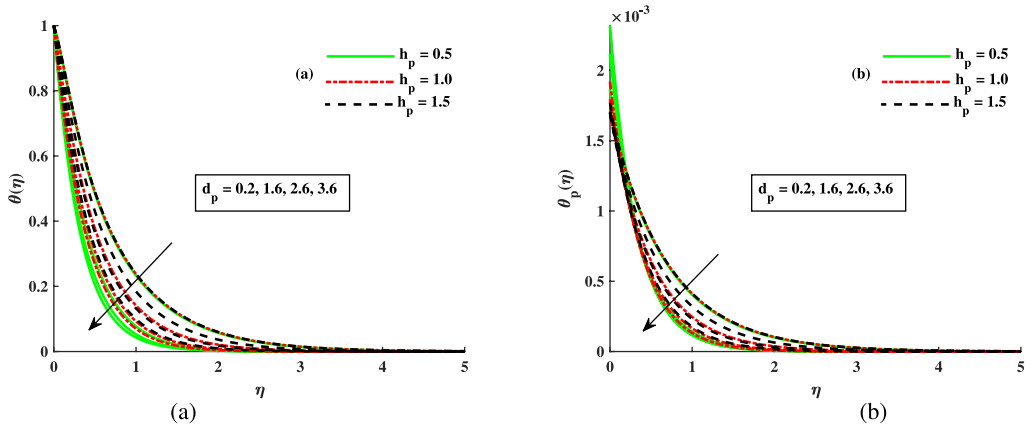

Fig. 5. Response of $\theta_p(\eta)$ and $\theta(\eta)$ for fluctuating h_p and d_p.

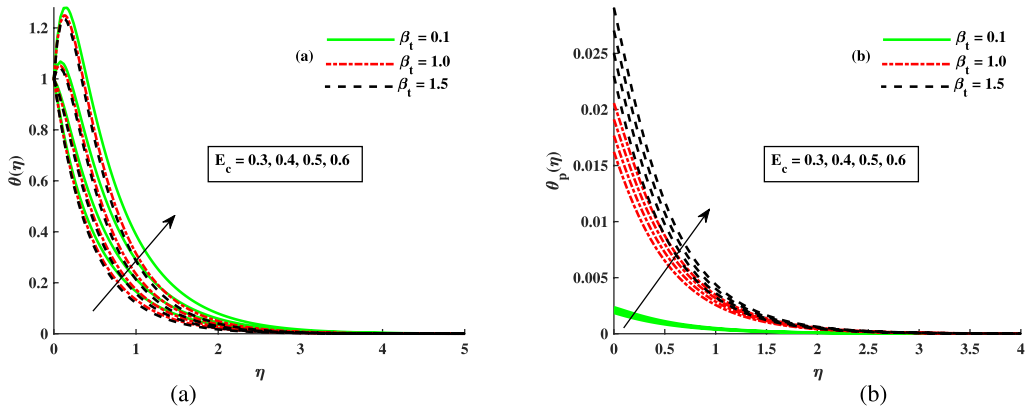

Fig. 6. Response of $\theta_p(\eta)$ and $\theta(\eta)$ for fluctuating E_c and β_t.

and Eckert number E_c on θ and θ_p. Higher β_t slows fluid motion and elevates dust-phase temperature due to enhanced thermal resistance. Elevated E_c represents viscous dissipation, directly raising both fluid and dust temperatures. These mechanistic interpretations guarantee significant insight by relating numerical results to physical processes.

Entropy generation and Bejan number

Entropy generation measures the degree of disorder, while the Bejan number distinguishes the entropy generated by heat transfer from the total entropy within a system. The second law of thermodynamics asserts that the entropy of an isolated system cannot decrease; hence, entropy generation is always non-negative. Figure 7(a) demonstrates that stronger magnetic fields enhance resistive heating and viscous dissipation, thereby increasing entropy generation. Conversely, decreasing the magnetic parameter reduces this resistive contribution, lowering total entropy generation. This reduction brings the system closer to its minimum irreversibility, which is fully in accordance with the second law of thermodynamics. Quantitatively, when the parameter M is raised from 1 to 5, the maximum entropy generation Ns at the wall increases by nearly 45%. An increase in Maxwell parameter β enhances Ns, as a higher relaxation time increases fluid-particle friction and heat loss. Quantitatively, increasing the Maxwell parameter β from 0.2 to 1 results in a nearly 40% increase in Ns. It highlights the role of viscoelastic relaxation time in amplifying heat loss and fluid-particle friction. Figure 7(b) further highlights that higher values of M and β lower the Bejan number Be, indicating a dominance of viscous dissipation over heat transfer. This trend shows a shift in the dominant source of irreversibility. At $\eta = 1.0$, the value of Be reduces from 0.85 to 0.45 as the magnetic parameter is elevated from 1 to 5, indicating a shift from heat-transfer-dominated irreversibility to a regime where viscous and magnetic effects contribute more than half of total entropy production.

Figure 8(a) visualizes that Ns increases with nanoparticle radius d_p but decreases with h_p. Larger particles impede conductive pathways and increase entropy, while smaller particles improve interfacial heat transfer, decrease irreversibility, and increase system efficiency due to their higher surface-area-to-volume ratios. Quantitatively, increasing d_p from 1.5 nm to 3.5 nm produces nearly a 30% rise in Ns. A key result of entropy minimization is that reducing d_p from 3.6 nm to 1.6 nm (a 2 nm decrease) under standard conditions ($\beta = 0.5$, $h_p = 0.5$, $M = 3$) reduces total entropy generation about 20%, confirming nanoparticle radius is a decisive parameter in controlling thermodynamic irreversibility. Increasing h_p reduces collisions, viscosity, and flow

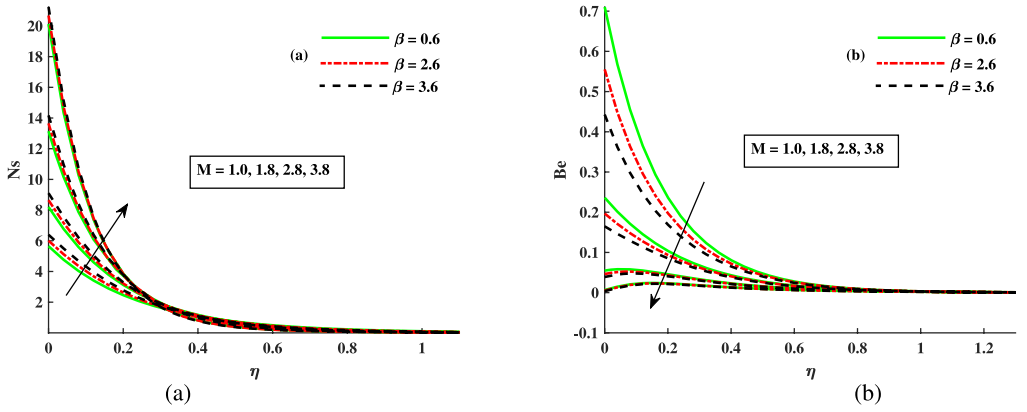

Fig. 7. Response of Ns and Be for fluctuating M and β.

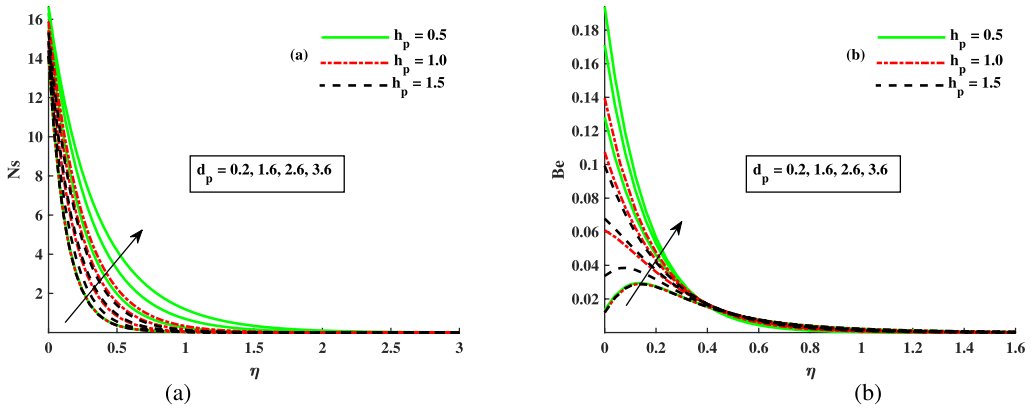

Fig. 8. Response of Ns and Be for fluctuating h_p and d_p.

blockage, thereby enhancing convective heat transport and decreasing entropy. Quantitatively, reducing h_p from 1.0 to 0.2 nearly doubles entropy due to viscous dissipation and enhanced clustering. Figure 8(b) shows that *Be* diminishes with h_p as convection becomes dominant, while larger d_p increases the Bejan number due to enhanced heat conduction. For $d_p = 1.5$ nm, *Be* remains above 0.8, confirming thermal transmission as the main irreversibility, whereas for $d_p = 3.5$ nm, it drops to about 0.6, indicating balanced contributions from other sources too. Optimizing h_p in material design enhances flow, heat transmission, and long-term performance. Pumps, pipelines, microelectronics, solar cooling, and other applications benefit from improved nanofluid stability, less friction, and increased energy efficiency when inter-particle spacing (h_p) is adjusted.

Figure 9(a) illustrates that entropy creation *Ns* grows with Eckert number E_c, reflecting the influence of viscous dissipation, while the thermal dusty parameter β_t enhances *Ns* by intensifying thermal resistance between the dust and fluid phases. Quantitatively, raising E_c from 0.1 to 0.5 increases maximum entropy generation by nearly 50%, underscoring its significant influence on system inefficiency. Figure 9(b) shows that *Be* decreases with E_c, falling to around 0.3 at $E_c = 0.5$, which indicates that 70% of the entropy arises from magnetic and viscous dissipation. In contrast, higher values of β_t increase *Be*, since stronger temperature gradients reinforce heat-transfer-dominated irreversibility. The findings emphasize on the role of E_c and β_t on improving energy efficiency and flow stability, with practical implications for the design of microelectronics, pipelines, and solar cooling systems.

Physical insights and applications

The numerical findings, though theoretical, carry direct industrial relevance. Clear mechanistic reasoning explains the observed trends: optimal inter-particle spacing minimizes clustering and viscous resistance, controlled magnetic fields improve flow stability, and viscous dissipation increases entropy. Smaller nanoparticles increase heat conduction by increasing surface-to-volume ratios, while proper interparticle spacing reduces flow resistance and clustering. Controlled magnetic fields enhance heat management and mitigate instabilities, but viscous dissipation increases entropy and reduces efficiency. The findings provide practical design recommendations for microelectronics, MHD power systems, solar collectors, and advanced cooling loops. They provide instructions for experimentalists and system designers pursuing energy-efficient and thermally stable solutions by connecting nanoscale particle attributes to macroscopic heat transfer efficiency and flow stability.

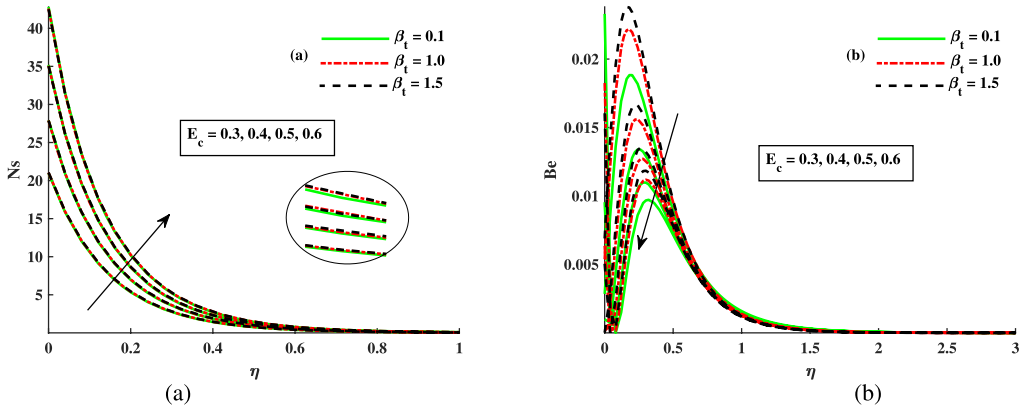

Fig. 9. Response of Ns and Be for fluctuating E_c and β_t.

Conclusion

This study numerically examined entropy generation in magnetohydrodynamic Maxwell dusty nanofluid flow across an inclined stretching sheet, with particular focus on the impacts of nanoparticle radius and inter-particle spacing. Unlike previous studies that largely overlooked these microstructural factors, our analysis highlights their role in entropy generation, dust-fluid interaction, and thermal conductivity. The governing equations were modified using similarity transformations and solved using MATLAB's bvp4c solver, revealing new insights into flow management, irreversibility, and thermal efficiency enhancement.

Key findings

- Intensified magnetic fields Lorentz forces, reducing velocities in both phases while increasing temperatures. This behavior applies to electromagnetic flow control devices and MHD pumps.
- Entropy generation and Bejan number rise with thermal dusty parameter β_t but have an inverse relationship with inter-particle spacing h_p, which affects cooling loops and pipeline design, where thermal efficiency is crucial.
- The Maxwell parameter improves flow resistance and energy dissipation while lowering the Bejan number, directly informing the design of viscoelastic nanofluids for cooling systems and solar collectors.
- Larger inter-particle spacing enhances thermal conduction while reducing velocity due to weaker particle interaction, providing design direction for nanofluids used in thermal exchangers.
- Fluid-dust momentum was increased by over 18% by nanoparticles larger than 2.5 nm, although thermal conductivity was lost by around 12%. This trade-off is especially important for microelectronics cooling, where flow must be sustained while minimizing heat loss.
- Entropy generation was suppressed by reducing the radius of the nanoparticle from 3.6 nm to 1.6 nm, which resulted in a reduction of irreversibilities of almost one-fifth. It shows a significant potential for energy-efficient working fluids in pipeline transport and solar cooling.
- A higher Eckert number raises temperature and entropy by increasing viscous dissipation but lowers the Bejan number, offering insights for high-speed fluid transport systems.

Limitations and future work

While this study gives valuable mechanistic insights, it depends on several simplifying assumptions. We investigated laminar flow with uniformly scattered nanoparticles, assuming that particle agglomeration is negligible, which may not accurately reflect real experimental situations. The findings are based on computational simulations rather than direct experimental validation; however, their dependability was validated through comparison with limiting cases. Furthermore, effects such as radiation, turbulence, and chemical reactions were excluded, even though they may be essential in large-scale industrial systems. Future research should address these challenges and incorporate experimental studies to support the current results.

Data availability

All the data used during this study are accessible within the manuscript.

Received: 9 August 2025; Accepted: 1 October 2025
Published online: 06 November 2025

References

1. Bejan, A. A study of entropy generation in fundamental convective heat transfer. *Journal of Heat Transfer* **101**(4), 718–725 (1979).
2. Bejan, A. & Kestin, J. Entropy generation through heat and fluid flow. *Journal of Applied Mechanics* **50**, 475–475 (1983).
3. Bejan, A. Entropy generation minimization: The new thermodynamics of finite-size devices and finite-time processes. *Journal of Applied Physics* **79**(3), 1191–1218 (1996).

4. Razaq, A., Khan, S. A., Alsaedi, A. & Hayat, T. Entropy induced flow model for solar radiation through nanomaterials with cubic autocatalysis reaction. *Journal of Magnetism and Magnetic Materials* **586**, 171172 (2023).
5. Sahoo, A. & Nandkeolyar, R. Entropy generation in magnetohydrodynamic radiative non-Darcy slip flow of a Casson nanofluid with Hall effects and activation energy. *Journal of Magnetism and Magnetic Materials* **575**, 170712 (2023).
6. Khan, S. A., Hayat, T., Razaq, A. & Momani, S. Entropy optimized flow subject to variable fluid characteristics and convective conditions. *Alexandria Engineering Journal* **86**, 616–630 (2024).
7. Saffman, P. On the stability of laminar flow of a dusty gas. *Journal of Fluid Mechanics* **13**(1), 120–128 (1962).
8. Ezzat, M. A., El-Bary, A. & Morsey, M. Space approach to the hydro-magnetic flow of a dusty fluid through a porous medium. *Computers & Mathematics with Applications* **59**(8), 2868–2879 (2010).
9. Abbas, Z., Hasnain, J. & Sajid, M. Effects of slip on MHD flow of a dusty fluid over a stretching sheet through porous space. *Journal of Engineering Thermophysics* **28**, 84–102 (2019).
10. Dey, D. & Chutia, B. Dusty nanofluid flow with bioconvection past a vertical stretching surface. *Journal of King Saud University-Engineering Sciences* **34**(6), 375–380 (2022).
11. Sharif, H. et al. Numerical investigation of dusty tri-hybrid Ellis rotating nanofluid flow and thermal transportation over a stretchable Riga plate. *Scientific Reports* **13**(1), 14272 (2023).
12. Alfvén, H. On the existence of electromagnetic-hydrodynamic waves. *Arkiv for Matematik, Astronomi och Fysik* **29**, 1–7 (1943).
13. Hayat, T., Qasim, M. & Mesloub, S. MHD flow and heat transfer over permeable stretching sheet with slip conditions. *International Journal for Numerical Methods in Fluids* **66**(8), 963–975 (2011).
14. Kumar, K. G., Gireesha, B. & Gorla, R. Flow and heat transfer of dusty hyperbolic tangent fluid over a stretching sheet in the presence of thermal radiation and magnetic field. *International Journal of Mechanical and Materials Engineering* **13**, 1–11 (2018).
15. Gireesha, B., Shankaralingappa, B., Prasannakumar, B. & Nagaraja, B. MHD flow and melting heat transfer of dusty Casson fluid over a stretching sheet with Cattaneo-Christov heat flux model. *International Journal of Ambient Energy* **43**(1), 2931–2939 (2022).
16. Ali, F. et al. Effects of Newtonian heating and heat generation on magnetohydrodynamics dusty fluid flow between two parallel plates. *Frontiers in Materials* **10**, 1120963 (2023).
17. Choi, S. U. & Eastman, J. A. Enhancing thermal conductivity of fluids with nanoparticles, (No. ANL/MSD/CP-84938; CONF-951135-29). Argonne National Lab.(ANL), Argonne, IL (United States) (1995).
18. Obalalu, A. M., Isarinade, A. F., Khan, U., Alsawah, G. A. & Hussain, S. M. Heat transfer enhancement in electroosmotic and ciliary-induced hybrid nanofluid flow with nonlinear thermal radiation effects. *Journal of Radiation Research and Applied Sciences* **18**(3), 101764 (2025).
19. Obalalu, A. M. et al. Electric double layer and thermal radiation effects on micropolar blood particles conveying Cu-MoS_2-CuO nanoparticles in squeezed arterial channel. *Nuclear Engineering and Technology* **57**(8), 103604 (2025).
20. Muhammad, K., Ahmed, B., Sharaf, M., Afikuzzaman, M. & Az-Zo'bi, E. A. Multiscale tribology analysis of MHD hybrid nanofluid flow over a curved stretching surface. *Nanoscale Advances* **6**(3), 855–866 (2024).
21. Alinejad, J. & Esfahani, J. A. Lattice Boltzmann simulation of 3-dimensional natural convection heat transfer of CuO/water nanofluids. *Thermophysics and Aeromechanics* **24**(1), 95–108 (2017).
22. Araban, H. P., Alinejad, J. & Ganji, D. D. Control temperature fluctuations in two-phase CuO-water nanofluid by transfiguration of the enclosures. *Thermal Science* **25**(1 Part B), 743–755 (2021).
23. Sahebi, S. A. R., Ganji, D. D. & Alinezhad, J. On the thermal performance of nanofluid over a cylinder within a confined channel: The splitter effect. *Case Studies in Thermal Engineering* **49**, 103275 (2023).
24. Timofeeva, E. V., Yu, W., France, D. M., Singh, D. & Routbort, J. L. Nanofluids for heat transfer: An engineering approach. *Nanoscale Research Letters* **6**, 1–7 (2011).
25. Madani, M. S. M., Alinejad, J., Rostamiyan, Y. & Fallah, K. Numerical study of geometric parameters effects on the suspended solid particles in the oil transmission pipelines. *Proceedings of the Institution of Mechanical Engineers, Part C: Journal of Mechanical Engineering Science* **236**(8), 3960–3973 (2022).
26. Hussain, M., Ali, B., Awan, A. U., Alharthi, M. & Alrashedi, Y. Role of nanoparticle radius for heat transfer optimization in MHD dusty fuid across stretching sheet. *Journal of Thermal Analysis and Calorimetry* 1–14 (2024).
27. Ali, B. et al. Significance of nanoparticle radius and gravity modulation on dynamics of nanofluid over stretched surface via finite element simulation: The case of water-based copper nanoparticles. *Mathematics* **11**(5), 1266 (2023).
28. Ali, B. et al. Significance of dust particles volume fraction to optimization of entropy in magnetohydrodynamic mixed convection flow via inclined surface. *Journal of Molecular Liquids* **394**, 123706 (2024).
29. Darvesh, A., Maiz, F. M., Santisteban, L. J. C., Anwar, T. & Almutairi, K. Particle size and inter-particle spacing effect on thermal performance of MHD copper nanofluid flow over dual-stretching rectangular frame: ANN-based simulations. *Case Studies in Thermal Engineering* 106682 (2025).
30. Ramzan, M. et al. Significance of nanoparticle radius and inter-particle spacing toward the radiative water-based alumina nanofluid flow over a rotating disk. *Nanotechnology Reviews* **12**(1), 20220501 (2023).
31. Algehyne, E. A. Dynamics of nanoparticle radius and inter-particle spacing on the nanofluid flow over an extending sheet with Cattaneo–Christov heat flux and inclined magnetic field impacts. *The European Physical Journal Plus* **139**(9), 802 (2024).
32. Lee, M.-H., Jeng, D. & Witt, K. D. Laminar boundary layer transfer over rotating bodies in forced flow. *Journal of Heat Transfer* **100**(3), 496–502 (1978).
33. Mahdy, A., Chamkha, A. J. & Nabwey, H. A. Entropy analysis and unsteady MHD mixed convection stagnation-point flow of Casson nanofluid around a rotating sphere. *Alexandria Engineering Journal* **59**(3), 1693–1703 (2020).
34. Biswas, R. et al. Computational treatment of MHD Maxwell nanofluid flow across a stretching sheet considering higher-order chemical reaction and thermal radiation. *Journal of Computational Mathematics and Data Science* **4**, 100048 (2022).
35. Hussain, M. et al. Characterization of thermal buoyancy forces and suction on bioconvective magnetohydrodynamic dusty nanofluid flow over a stretching surface. *Modern Physics Letters B* 2550209 (2025).
36. Akbar, A. A. et al. Magnetized heat transfer visualization through computational modeling of third-grade fluid via exponentially stretching cylinder. *Modern Physics Letters B* 2450334 (2024).
37. Khan, M. N. et al. Theoretical study on thermal efficiencies of Sutterby ternary-hybrid nanofluids with surface catalyzed reactions over a bidirectional expanding surface. *Journal of Molecular Liquids* **391**, 123412 (2023).
38. Galal, A. M. et al. Impact of buoyancy forces and electroosmosis in a peristaltic transport of a non-Newtonian tri-hybrid nanofluid induced by an asymmetric channel. *Journal of Thermal Analysis and Calorimetry* 1–18 (2025).
39. Afridi, M. I., Qasim, M., Khan, I., Shafie, S. & Alshomrani, A. S. Entropy generation in magnetohydrodynamic mixed convection flow over an inclined stretching sheet. *Entropy* **19**(1), 10 (2016).
40. Graham, A. L. On the viscosity of suspensions of solid spheres. *Applied Scientific Research* **37**, 275–286 (1981).
41. Gosukonda, S., Gorti, V. S., Baluguri, S. B. & Sakam, S. R. Particle spacing and chemical reaction effects on convective heat transfer through a nano-fluid in cylindrical annulus. *Procedia Engineering* **127**, 263–270 (2015).
42. Ali, B. et al. Significance of Lorentz and Coriolis forces on dynamics of water based silver tiny particles via finite element simulation. *Ain Shams Engineering Journal* **13**(2), 101572 (2022).
43. Awan, A. U. et al. Computational analysis of entropy generation in EMHD micropolar dusty fluid flow incorporating esterification process. *Scientific Reports* **15**(1), 30146 (2025).

44. Panda, S., Shamshuddin, M. D., Obalalu, A. M., Salawu, S. O. & Mishra, S. R. Cattaneo-Christov hypothesis in a micropolarnanofluid flow over a stretching sheet subjected to exponential space-based heat generation and bilateral reactions. *Case Studies in Thermal Engineering* 106813 (2025).
45. Jalil, M., Asghar, S. & Yasmeen, S. An exact solution of MHD boundary layer flow of dusty fluid over a stretching surface. *Mathematical Problems in Engineering* **2017**(1), 2307469 (2017).
46. Rehman, S. U. et al. The Casson dusty nanofluid: Significance of Darcy–Forchheimer law, magnetic field, and non-Fourier heat flux model subject to stretch surface. *Mathematics* **10**(16), 2877 (2022).

Acknowledgements
The authors extend their appreciation to the Deanship of Research and Graduate Studies at King Khalid University for funding this work through Large Research Project under grant number RGP2/403/46.

Author contributions
A.U.A.: Supervision; writing and editing. S.Niazai: Data curation; Visualization. M.H.: Formal Analysis; Writing original manuscript. B.A.: Conceptualization; Methodology. N.A.A.: Resources; Data Curation. F.G.: Software; Investigation. S.Nadeem: Validation; Project administration.

Declarations

Ethical approval
The authors affirm their commitment to ethical standards.

Conflicts of interest
There are no conflicts of interest to declare.

Additional information
Correspondence and requests for materials should be addressed to S.N.

Reprints and permissions information is available at www.nature.com/reprints.

Publisher's note Springer Nature remains neutral with regard to jurisdictional claims in published maps and institutional affiliations.